

# Comparison Between Theoretical CFV Flow Models and NIST's Primary Flow Data in the Laminar, Turbulent, and Transition Flow Regimes

Aaron Johnson

e-mail: aaron.johnson@nist.gov

John Wright

National Institute of Standards and Technology  
(NIST),  
100 Bureau Drive,  
Mail Stop 8361,  
Gaithersburg, MD 20899

*State-of-the art dimensional metrology was used to measure the throat diameter and throat curvature of nine critical flow venturis (CFVs) with nominal throat diameters ranging from 5 mm to 25 mm. The throat curvature was used in calculating the theoretical discharge coefficients, while the throat diameter was used in computing the experimental discharge coefficients. The nine CFVs were calibrated in dry air using two NIST primary flow standards with expanded uncertainties of 0.05% and 0.09%, respectively. The calibration data span a Reynolds number range from  $7.2 \times 10^4$  to  $2.5 \times 10^6$ , including laminar, transition, and turbulent flow regimes. By correcting for both the throat diameter and curvature, the agreement between predicted and measured discharge coefficients was less than 0.17% in the turbulent regime and less than 0.07% in the laminar regime. [DOI: 10.1115/1.2903806]*

## Introduction

Critical flow venturis (CFVs) are widely used in the flow metering community as flow meters, check standards, and transfer standards. The popularity of these devices is a result of their excellent long term reproducibility [1], simple geometric design [2], straightforward application, and well understood physics. Much of the pioneering work for CFV flowmeters was done during the 1960s and 1970s when numerous theoretical flow models were developed for predicting the CFV discharge coefficient. Recent calibration data taken in air by Ishibashi [3–6] quantified the accuracy of these models over a portion of the laminar flow regime. Ishibashi's measurements of the discharge coefficient agreed with theoretical predictions to better than 0.03% over a Reynolds numbers range from  $8 \times 10^4$  to  $2.5 \times 10^5$ . For this comparison, he used *high precision nozzles* (HPNs), manufactured on ultrahigh precision lathes, whose throat diameters ( $d$ ) are known to better than a fraction of a micron and whose throat radius of curvature ( $r_c$ ) and overall CFV profiles match the ISO [2] recommended shape to better than  $1 \mu\text{m}$ . Consequently, HPNs come closest of any manufactured CFV to the ideal nozzle shape and are the best choice for comparing measured versus predicted values of the discharge coefficient.

Unfortunately, for CFV theorists, the high cost of HPNs, which is nearly ten times that of a normally manufactured CFV, significantly reduces their use within the flow metering community. By normally manufactured, we mean produced on something less than an ultrahigh precision lathe and generally polished after machining. For practical reasons, it is of interest to determine how well the discharge coefficients of normally manufactured CFVs compare with theoretically predicted values.

In this work, NIST characterized both the flow performance and geometry of nine normally manufactured CFVs. The nominal

CFV throat diameters ranged from 5 mm to 25 mm, and the Reynolds numbers extended from  $7.2 \times 10^4$  to  $2.5 \times 10^6$ . The flow calibrations were done in dry air using two pressure-volume-temperature-time (PVTt) primary flow standards [7–10]. NIST's Moore M48 coordinate measuring machine was used to determine the CFV contours [11], from which we determined the throat diameter, and the throat curvature ratio ( $\Omega \equiv d/2r_c$ ). Other geometric features that were qualitatively assessed include the degree of eccentricity and twist of the various cross sections along the CFV centerline.

The measured  $d$ 's were used in calculating the experimental discharge coefficients ( $C_{d,\text{exp}}$ ), while  $\Omega$ 's were used in calculating the predicted discharge coefficients ( $C_{d,\text{th}}$ ). Figure 1 shows that the overall agreement between  $C_{d,\text{exp}}$  and  $C_{d,\text{th}}$  is better than 0.17% over a Reynolds number range extending from  $7.2 \times 10^4$  to  $2.5 \times 10^6$ . This good agreement is surprising since no effort was made to model the boundary layer transition from laminar to turbulent flow. Instead, we implemented a simple piecewise model that assumed laminar flow for Reynolds numbers below  $10^6$  and turbulent flow at higher Reynolds numbers.

The theoretically predicted discharge coefficient ( $C_{d,\text{th}}$ ) is obtained using a composite model consisting of three submodels. Each submodel accounts for different physical phenomena including boundary layer development along the CFV wall, curvature of the sonic line at the CFV throat, and departure from ideal gas behavior (i.e., virial effects). In general, these three mechanisms characterize the discharge coefficient of CFV flows. Other secondary mechanisms affecting the discharge coefficient, such as swirl, heat transfer, and vibrational relaxation, are made insignificant by selecting the appropriate gases and flow conditions (i.e., swirl free dry air at near ambient temperature). We use experimental data to assess the accuracy of several of the commonly used submodels, and we introduce a systematic approach based on a Taylor series expansion method to combine the three submodels into a single composite model for predicting  $C_{d,\text{th}}$ . The Taylor series method is also used to estimate errors in  $C_{d,\text{exp}}$  attributed to species dependent virial effects. These errors are inherent in the present definition of the discharge coefficient, which attempt to eliminate the

Contributed by the Fluids Engineering Division of ASME for publication in the JOURNAL OF FLUIDS ENGINEERING. Manuscript received August 16, 2006; final manuscript received May 18, 2007; published online July 22, 2008. Assoc. Editor: James A. Liburdy.

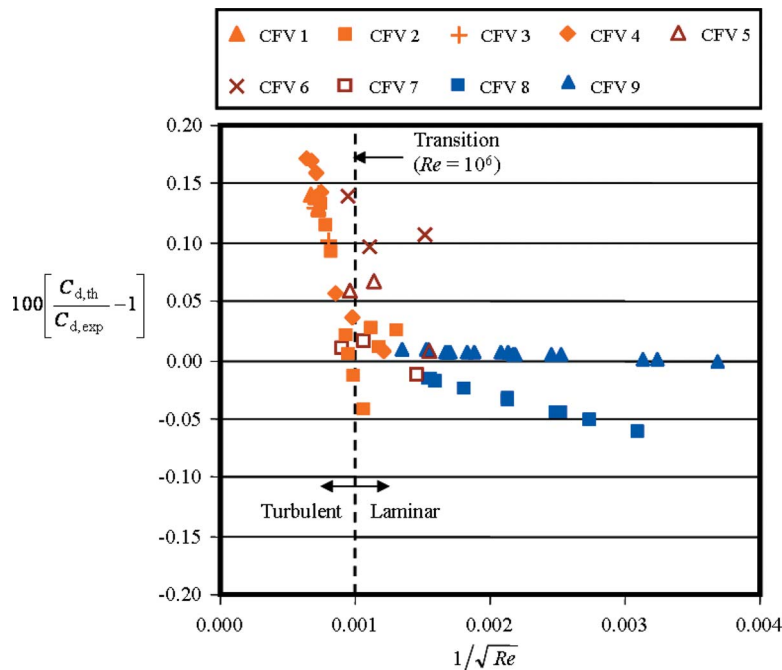


Fig. 1 Percent difference between theoretical models and experimental data for nine normally manufactured CFVs

influence of virial effects so that  $C_{d,exp}$  is primarily dependent on Reynolds number alone. These errors must be considered whenever a CFV is calibrated in one gas, but the calibration curve is applied using a different gas.

### PVTt Flow Standards and the Historical Calibration Records of CFVs

The two NIST PVTt flow standards used to calibrate the CFVs have nominal collection tank volumes of 677 l and 26 m<sup>3</sup>, respectively. Together, these PVTt systems cover a flow range extending from 100 l/min to 78,000 l/min.<sup>1</sup> The two smallest CFVs were calibrated using both the 677 l PVTt flow standard and the 26 m<sup>3</sup> PVTt flow standard. The remaining seven CFVs were calibrated using only the 26 m<sup>3</sup> PVTt standard. For all of the calibrations, the CFV stagnation temperature was maintained close to room temperature while the stagnation pressure ranged from 150 kPa to 850 kPa. The expanded mass flow uncertainties for the 677 l and 26 m<sup>3</sup> PVTt systems are 0.05% [7,8] and 0.09% [9,10], respectively.

Table 1 shows the calibration history for the set of nine CFVs. For convenience, each CFV is identified by the numerical value in Column 1 throughout this document. Column 2, gives the total number of calibration points (where the number of calibrations is in parentheses), Column 3 provides the standard deviation of residuals between a best fit curve of all the calibration data and the measured discharge coefficients, and Column 4 gives the relative uncertainty of the measured discharge coefficients (where the values in parentheses are the uncertainties obtained on the 677 l PVTt standard). Altogether, the calibration records contain 1007 data points.

The largest source of uncertainty in the discharge coefficient stems from the PVTt mass flow measurements. Other factors including the stagnation pressure, stagnation temperature, critical flow factor, throat diameter, etc., also contribute to the uncertainty

so that the uncertainty of the discharge coefficient is slightly above the uncertainty of the mass flow. The uncertainty of CFV 6 is larger than its counterparts since all of its calibration data pre-date 2003, when performance upgrades reduced the uncertainty of the 26 m<sup>3</sup> PVTt flow standard from 0.21% to 0.09% [10].

### Dimensional CFV Measurements

The throat diameter ( $d$ ) and the throat curvature ratio ( $\Omega$ ) are the key geometric parameters for comparing measured and predicted values of the discharge coefficient. In a routine calibration, the discharge coefficient can be calculated using only a nominal value of the throat diameter. In this case, any error in diameter uniformly shifts the calibration curve above or below its true value, but the offset is compensated when the calibration curve is used to compute the mass flow provided the same nominal diameter is used. In fact, it is common to obtain measured discharge coefficients that exceed unity when  $C_{d,exp}$  is calculated using a nominal diameter that is less than the actual diameter. However,

Table 1 Calibration history for selected CFVs using dry air as the working fluid

CFV No.	No. of points (No. of cal)	Std. dev. of best fit residuals ( $\times 10^6$ )	Rel. unc. of discharge coefficient ( $k=2$ ) (%)
1	37 (1)	80	0.11
2	79 (1)	170	0.11
3	42 (1)	137	0.11
4	62 (1)	68	0.11
5	150 (3)	405	0.11
6	60 (2)	482	0.21
7	90 (3)	460	0.11
8	234 (4)	300	0.11 (0.08)
9	253 (4)	290	0.11 (0.08)

<sup>1</sup>Unless otherwise noted, all volumetric flows in this paper are taken to be at standard conditions with a temperature at 293.15 K and a pressure of 101.325 kPa.

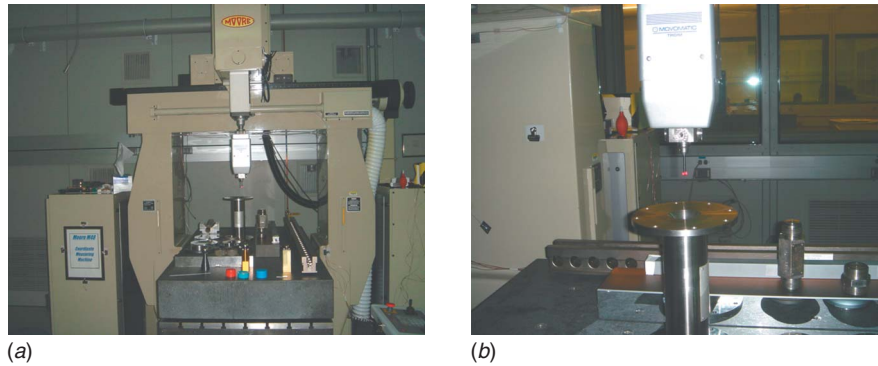


**Fig. 2 Moore M48 CMM (the left picture shows a full view of CMM while the right one shows a close-up of probe and CFV just prior to dimensional calibration)**

any offset in  $C_{d,exp}$  is undesirable when comparing measured to predicted values of the discharge coefficient, and therefore highly accurate values of  $d$  are necessary. For example, since the discharge coefficient is proportional to the diameter squared, a diameter uncertainty of 0.05% leads to a 0.1% uncertainty in the measured discharge coefficient. On the other hand, the theoretical discharge coefficient is not strongly dependent on  $\Omega$ , and relatively large uncertainties can be tolerated. For the Reynolds number range considered in this paper, an uncertainty of 10% or less is acceptable to ensure an effect of less than 0.02% on the predicted discharge coefficient.

Figure 2 shows pictures of NIST's Moore M48 coordinate measuring machine (CMM). This machine is commonly regarded as one of the most accurate CMMs in the world, capable of making position measurements with uncertainties as low as  $0.05 \mu\text{m}$ . In this application, the uncertainty of throat diameter measurements is  $0.5 \mu\text{m}$  (i.e., for  $k=1$ ). This machine is housed in a temperature controlled environment that is maintained at  $(20 \pm 0.01)^\circ\text{C}$  to provide superior thermal stability. Moreover, the machine's heavy supporting structure gives it excellent mechanical stability. Detailed descriptions explaining the construction and operating principle of the Moore M48 can be found in Ref. [11].

Both  $d$  and  $\Omega$  are indirectly determined by probing along the circumference of various cross sections and measuring contours along different azimuthal planes of symmetry. The contours of the CFVs are determined by traversing the probe of the Moore M48 along the nozzle wall through the throat region. At each cross section, the probe makes 12 radial measurements spaced 30 deg apart. These 12 measurements are used to calculate the cross sectional area. In this work, the cross sectional area is estimated by fitting the *best fit* ellipse through the 12 points. The ellipsoidal fit accounts for eccentricity observed in some of the CFVs but collapses to a circle in the special case where the data are perfectly round. By dividing the area determined by the ellipsoidal fit by  $\pi$  and taking its square root, we determine the *effective* radius at each cross section. The average CFV contour was estimated by fitting the measured data to either a fifth or sixth degree polynomial that expressed the calculated radius as a function of axial position. The axial position of the throat is determined by setting the derivative of the polynomial equal to zero. The throat diameter equals twice the value of the polynomial evaluated at the axial throat location, and the throat curvature equals the second derivative of the polynomial evaluated at the throat location.

Figure 3 shows the cross sectional shapes for all nine CFVs at five axial positions traversing the throat. At each axial location, the deviation from circularity (in microns) was calculated by taking the difference between the 12 radial measurements and the calculated average radius. For comparison purposes, all of the plots have the same scaling, varying from  $-15 \mu\text{m}$  to  $10 \mu\text{m}$ . The

figure shows that CFV 8 significantly deviates from the circular shape while the remaining CFVs are essentially circular. In addition, the cross sectional shapes of all the CFVs remain relatively consistent along the axis of symmetry (i.e., negligible twisting).

Figure 4 shows the near throat profiles of the nine CFVs (i.e., plots of the polynomial fits). The various profiles are labeled with the measured values of  $\Omega$  where the subscripts identify the CFV. The shaded region in the figure shows the recommended range of curvature ratios for an ISO CFV. For CFVs 1–4, 8, and 9, the measured  $\Omega$  is less than the minimum requirement given by the ISO standard. We hypothesize that polishing the throat flattens the profile, causing smaller  $\Omega$  in the region close to the throat. In the Results section, we show that predicted  $C_d$  values that are calculated with the measured values of  $\Omega$  generally have better agreement with measured data than those calculated using an assumed ISO value of  $\Omega_{ISO}=0.25$ .

Table 2 shows the throat diameter, the throat curvature ratio, and their expanded relative uncertainties (i.e.,  $k=2$ ) for all nine CFVs. The uncertainties of the throat diameters are calculated by root sum squaring the  $0.5 \mu\text{m}$  ( $k=1$ ) uncertainty of the CMM measurements and the uncertainty attributed to the eccentricity of the CFV cross section. The standard uncertainty attributed to eccentricity is taken to be proportional to the absolute difference of two throat radii, calculated by two different methods. In one case, the best fit ellipse (as previously explained) is used to determine the effective radius, while in the other case, the best fit circle is used. Since we expect the uncertainty to fall between these two radii, a rectangular distribution is assumed and the standard uncertainty is taken equal to the absolute difference of the two radii divided by  $\sqrt{3}$  [12,13]. For all these CFVs (with the exception of CFV 8), the effect of eccentricity is negligible.

The ellipsoidal shape of CFV 8 results in a strong angular dependence of its curvature ratio. The uncertainty of the throat curvature ratio is equal to the standard deviation the twelve  $\Omega$  determinations of  $\Omega$ , each calculated along one of the 12 contours spaced 30 deg apart.

### CFV Principle of Operation and Physics

Figure 5 shows an axisymmetric cut of a toroidal shaped CFV with dimensions complying with the ISO 9300 standard [2]. The CFV profile consists of a circular arc extending slightly beyond the throat cross section to a point of tangency, followed by a conical divergent section with a half angle between 2 deg and 6 deg. When sufficient pressure ratios (i.e.,  $P_b/P_0$ ) exist across the CFV, the gas flow achieves sonic velocity near the throat. Here,  $P_0$  is the upstream stagnation pressure and  $P_b$  is the static

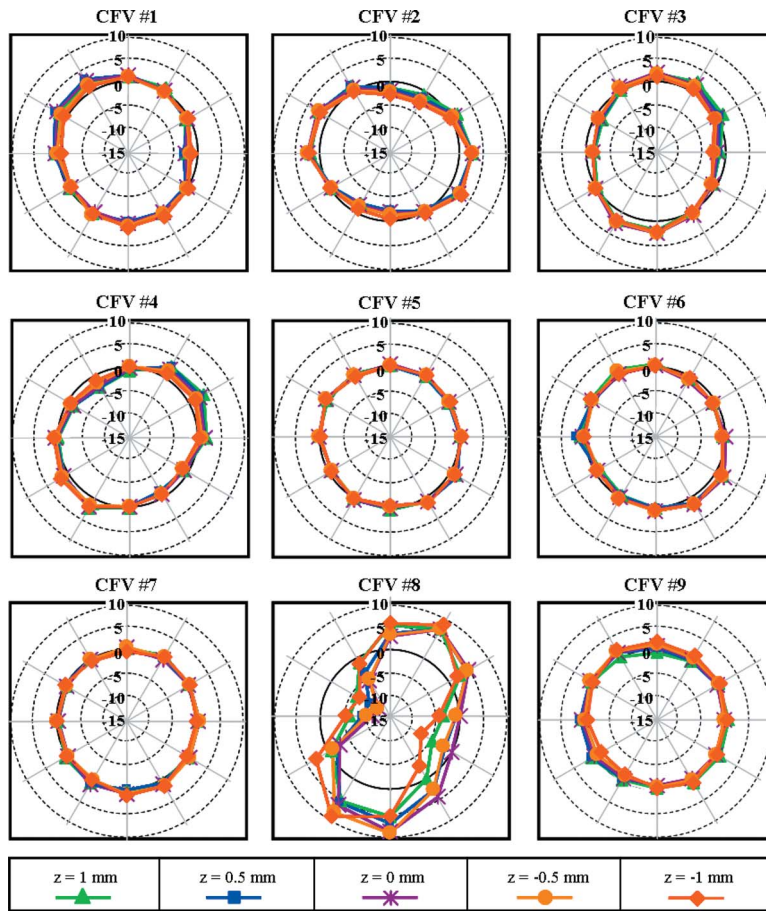


Fig. 3 Degree of roundness (in microns) for CFVs at five axial positions traversing the throat cross section (positive axial values correspond to positions upstream of the throat while negative values correspond to positions downstream of the throat)

pressure downstream of the CFV exit. The largest pressure ratio that satisfies this condition is called the *choking pressure ratio* (CPR) and CFVs are operated at or below this value.

Under choked flow conditions (i.e.,  $P_b/P_0$  less than the CPR), the CFV mass flow is independent of the thermodynamic conditions downstream of the throat section. Physically, pressure fluctuations

cannot propagate upstream of the sonic throat.<sup>2</sup> Consequently, the mass flow is proportional to the upstream stagnation

<sup>2</sup>In small CFVs, the mass flow could exhibit some dependence on  $P_b$  attributed to pressure disturbances propagating upstream via the subsonic boundary layer.

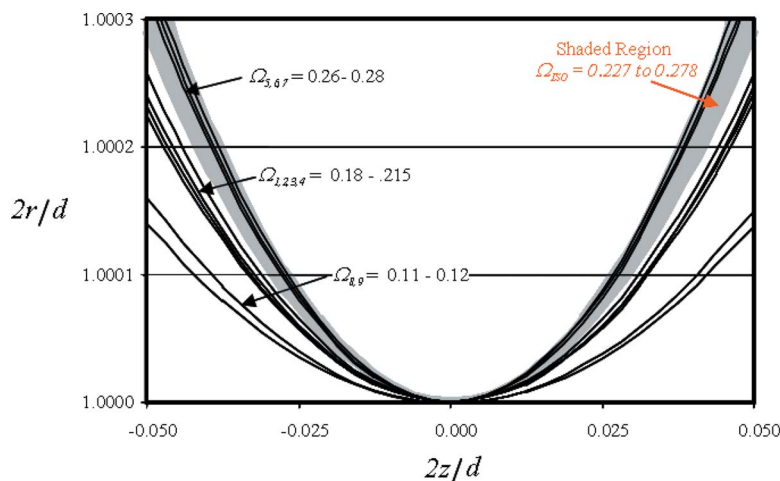


Fig. 4 Near throat CFV profiles (the shaded region indicates the ISO recommended values of the throat curvature ratio)

**Table 2 Measured values of throat diameter ( $d$ ) and curvature ratio ( $\Omega$ ) and their relative uncertainties ( $k=2$ )**

CFV No.	$d$ (mm)	$\left[\frac{U(d)}{d}\right]$ (%)	$\Omega$	$\left[\frac{U(\Omega)}{\Omega}\right]$ (%)
1	25.3928	0.004	0.215	6.0
2	25.3912	0.004	0.19	8.1
3	25.3933	0.004	0.205	8.4
4	25.3884	0.004	0.18	7.4
5	19.7517	0.005	0.26	1.6
6	18.7857	0.005	0.265	2.9
7	17.3489	0.006	0.28	2.4
8	6.3784	0.020	0.12	51.7
9	4.8284	0.021	0.11	9.4

pressure alone, in contrast to a venturi operating at subsonic conditions where the flow is proportional to the difference between the upstream and downstream pressures.

Quantitative predictions of the CFV mass flow are commonly obtained via the published theoretical models [14–24]. The complexity as well as the accuracy of these models can significantly vary. The simplest of these models provides a common basis for all of the more sophisticated models and is herein called the *base line* model. The base line model is derived by reducing the Navier–Stokes equations [25] using the following three assumptions.

- (1) The flow is one dimensional.
- (2) The flow processes are isentropic.
- (3) The fluid is a calorically perfect gas (i.e., the compressibility factor equals one and the constant pressure heat capacity is constant).

Together, Assumptions (1)–(3) are herein called the *sonic assumption*. Under the sonic assumption, the base line CFV mass flow is [14]

$$\dot{m}_b = \frac{\pi d^2 P_0 C_i^* \sqrt{\mathcal{M}}}{4 \sqrt{R_u T_0}} \quad (1)$$

where  $P_0$  is the upstream stagnation pressure,  $T_0$  is the upstream stagnation temperature,  $R_u$  is the universal gas constant,  $\mathcal{M}$  is the molecular weight, and  $C_i^*$  is the *ideal* gas critical flow function

$$C_i^* = \sqrt{\gamma} \left[ \frac{\gamma + 1}{2} \right]^{(\gamma + 1)/2(1 - \gamma)} \quad (2)$$

where  $\gamma = C_p/C_v$  is the specific heat ratio evaluated at the upstream static pressure and temperature.

The sonic assumption typically leads to predicted mass flows that agree with measurements to much better than 5% of the actual value (primarily depending on Reynolds number). However, the sonic assumption is not fully satisfied in actual CFV flows primarily for three reasons.

- (1) The boundary layer. The isentropic assumption is not valid in the boundary layer adjacent to the CFV wall. In this region, viscous effects retard the fluid motion, thereby reducing the gas velocity below the sonic velocity. Simultaneously, shear between adjacent fluid layers heat the gas, leading to larger temperatures, and subsequently lower densities than the fluid density in the inviscid core beyond the boundary layer. Together, the lower velocity and lower density lead to the decreased mass flow through the boundary layer region than would be predicted by the base line model.
- (2) The inviscid core. The flow in the center, beyond the boundary layers, is multidimensional so that the profile of the sonic line (i.e., locus of points where the Mach number is unity) is nearly parabolic instead of the flat profile predicted by the base line model. The effect of the curved sonic line is to reduce the mass flow in the core region below the base line model.
- (3) Virial effects. Real gas effects alter both the sound speed and the density, causing them to differ from the values predicted for a perfect gas with a constant heat capacity. In this case, virial effects can either increase or decrease the CFV mass flow depending on the upstream stagnation conditions and gas specie.

For the past 40 years, researchers have analyzed these three phenomena and developed corrections to the base line model, resulting in the state-of-the-art theoretical models that predict CFV performance. We compare our experimental data to these theoretical models. It should be noted that other phenomena, notably, vibrational relaxation [26] and heat transfer from the CFV wall, are also significant in many cases, but they have not yet been incorporated into the theoretical models due to their complexity.

In practice, the base line mass flow is used as the normalizing parameter in the definition of the ideal discharge coefficient

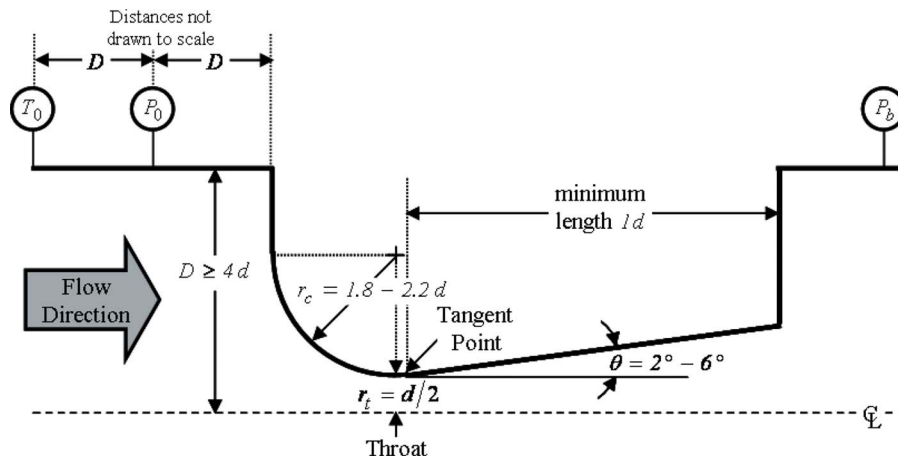


**Fig. 5 Axisymmetric cut of a toroidal shaped CFV with dimension specifications of the ISO 9300 standard [2]**

$$C_d^i \equiv \frac{\dot{m}}{\dot{m}_b} = \frac{4\dot{m}\sqrt{R_u T_0}}{\pi d^2 P_0 C_i^* \sqrt{\mathcal{M}}} \quad (3)$$

where  $\dot{m}$  is either measured or determined theoretically, and the superscript  $i$  distinguishes the ideal discharge coefficient from the real discharge coefficient. The real discharge coefficient is indicated by the superscript  $r$  and is defined by

$$C_d^r \equiv \frac{4\dot{m}\sqrt{R_u T_0}}{\pi d^2 P_0 C_r^* \sqrt{\mathcal{M}}} = \left( \frac{C_i^*}{C_r^*} \right) C_d^i \quad (4)$$

replacing the *ideal gas* critical flow factor ( $C_i^*$ ) with the *real gas* critical flow factor ( $C_r^*$ ). The details explaining how to calculate  $C_r^*$  for various gases are given in Ref. [20]. In general, the real discharge coefficient ( $C_d^r$ ) is preferred over the ideal discharge coefficient ( $C_d^i$ ) for the following three reasons.

- (1) The value of the real gas discharge coefficient is always less than unity,  $C_d^r < 1$ ,<sup>3</sup> while in contrast, virial effects could potentially result in  $C_d^i > 1$ .
- (2)  $C_d^r$  is nearly independent of real gas effects so that the discharge coefficient of different gases will be identical regardless of the degree of virial effects, provided that the set of dimensionless variables characterizing the discharge coefficient of both gases are all identical.
- (3) In the absence of virial effects, the real gas critical flow function equals the ideal value (i.e.,  $C_r^* \rightarrow C_i^*$ ) and both definitions of the discharge coefficient are identical.

For these reasons,  $C_d^r$  is used instead of  $C_d^i$  unless otherwise noted for all measurements of the discharge coefficient. Consequently, the superscript  $r$  is omitted in the real gas discharge coefficient and it is expressed as  $C_d$ . For the thermodynamic range considered in this analysis, Condition (3) nearly realized so that  $C_i^*$  can be used in the place of  $C_r^*$  with negligible error (i.e., less than 0.01%).

In general, the discharge coefficient is a function of several variables including the Reynolds number, the specific heat ratio, heat transfer effects at the CFV wall, etc. A complete list of all of the pertinent dimensionless parameters characterizing the discharge coefficient is given in Ref. [27]. However, among the numerous parameters influencing the discharge coefficient, the Reynolds number is usually the most important. This fact has been demonstrated by numerous calibration data and by the various theoretical models. A commonly used Reynolds number definition is

$$\text{Re} = \frac{4\dot{m}_b}{\pi d \mu_0} \quad (5)$$

where  $\mu_0$  is the molecular viscosity evaluated at the upstream stagnation conditions. An alternative Reynolds number definition also commonly used in the literature replaces the base line mass flow  $\dot{m}_b$  in Eq. (5) with the measured mass flow  $\dot{m}$ . Although either definition is acceptable, we use the definition in Eq. (5) throughout this paper.

## Review of Existing Theoretical Models

Although numerous theoretical models have been formulated to predict the discharge coefficient, no single model has been developed that simultaneously eliminates all three conditions of the sonic assumption. Instead, three distinct types of theoretical models have been developed, each focusing on improving a single

<sup>3</sup>Here, we assume that the discharge coefficient is calculated using the actual CFV throat diameter and that the mass flow is not affected by nontraditional mechanisms such as vibrational relaxation phenomena observed for CO<sub>2</sub> and SF<sub>6</sub> in geometrically small CFVs [26,27].

aspect of the sonic assumption. This has resulted in three distinct definitions of theoretical discharge coefficients including

- (1) the viscous discharge coefficient  $C_{d,1}$
- (2) the inviscid discharge coefficient  $C_{d,2}$ , and
- (3) the virial discharge coefficient  $C_{d,3}$

which are herein distinguished by the subscripts 1, 2, and 3, respectively. Each of these three discharge coefficients results from a different simplification of the Navier–Stokes equations. In particular,  $C_{d,1}$  is derived by retaining Conditions (2) and (3) of the sonic assumption, but modifying Condition (1) to account for the boundary layer development along the CFV wall. In a similar manner,  $C_{d,2}$  (and  $C_{d,3}$ ) modifies the second (and third) condition of the sonic assumption while enforcing the remaining two. Each model is explained below.

## Viscous Discharge Coefficient ( $C_{d,1}$ )

The viscous discharge coefficient accounts for the boundary layer development along the CFV wall. Predictive models have been developed both for laminar [15,16] and for turbulent flows [17]. For a smooth CFV contour, the boundary layer transition from the laminar to the turbulent flow typically occurs within a Reynolds number range extending from  $8 \times 10^5$  to  $1.8 \times 10^6$ . The transition, however, has been observed at significantly lower Reynolds numbers in CFVs with rough walls. In this work, all of the CFVs have sufficiently smooth walls so that the transition to the turbulent flow occurs within the normal Reynolds number regime.

Among the various laminar flow models, the two most sophisticated and accurate models were independently developed by Tang in 1969 and by Geropp in 1971. Both of these models used similarity transformations to solve the axisymmetric compressible boundary layer equations. The turbulent flow model was developed in 1964 by Stratford who used an integral boundary layer technique to determine the turbulent displacement thickness and subsequently the viscous discharge coefficient. For either laminar or turbulent flow, the viscous discharge coefficient has the following form:

$$C_{d,1} = 1 - a_1 \Omega^{-m} \text{Re}^{-n} + a_2 \Omega^{-2m} \text{Re}^{-2n} \quad (6)$$

where  $a_1$  and  $a_2$  are coefficients, and  $m$  and  $n$  are exponents whose values depend on whether the flow is laminar or turbulent. Table 3 gives the values of these coefficients and exponents for the various models. The viscosity ratios ( $\mu^*/\mu_0$ ) in both Tang's and Stratford's model convert between the Reynolds number definition based on the stagnation molecular viscosity ( $\mu_0$ ) given in Eq. (5) and the Reynolds number based on the molecular viscosity evaluated at the CFV throat ( $\mu^*$ ) that was used in these models. The coefficients  $a_1$  and  $a_2$  were calculated using a nominal value of the specific heat ratio for dry air ( $\gamma=1.405$ ). No attempt was made to account for the slight variation in  $\gamma(P, T)$  attributed to different CFV operating conditions (i.e., different pressures and temperatures at the CFV inlet). The change in  $C_{d,1}$  attributed to the slight variation in  $\gamma$  was less than 0.006% and taken to be negligible for the range of Reynolds numbers considered in this work.

For CFV flows with Reynolds number larger than  $10^4$ , the last term in Eq. (6) is small relative to the other terms and is often omitted. For example, for the Reynolds number range considered in this paper, this term accounts for less than 0.005% of  $C_{d,1}$ . Consequently, the measured discharge coefficient scales almost linearly with  $\text{Re}^{-1/2}$  in the laminar flow regime.

In this work, the viscosity ratios ( $\mu^*/\mu_0$ ) in the coefficients  $a_1$

**Table 3 Coefficient and exponent for selected boundary layer models used for predicting  $C_{d,1}$ <sup>a</sup>**

Viscous solutions for $C_{d,1}$	Flow type	Exponents		Coefficients	
		$m$	$n$	$a_1$	$a_2$
Tang [15]	Laminar	1/4	1/2	$2 \left[ \frac{\gamma\sqrt{2+6\sqrt{3}-7\sqrt{2}}}{\sqrt{3}} \right] \left( \frac{\gamma+1}{2} \right)^{-1/4} \left( \frac{\mu^*}{\mu_0} \right)^{1/2}$	$\left[ \frac{2\sqrt{2}(\gamma-1)(\gamma+2)}{3\sqrt{\gamma+1}} \right] \left( \frac{\mu^*}{\mu_0} \right)$
Geropp [16]	Laminar	1/4	1/2	$2 \left[ \frac{\gamma\sqrt{2+6\sqrt{3}-7\sqrt{2}}}{\sqrt{3}} \right] \left( \frac{\gamma+1}{2} \right)^{-3/4}$	$\left[ \frac{\gamma\sqrt{2+6\sqrt{3}-7\sqrt{2}}}{\sqrt{3}} \right]^2 \left( \frac{\gamma+1}{2} \right)^{-3/2}$
Stratford [17]	Turbulent	2/5	1/5	$\left( \frac{21}{400} \right) \left( \frac{1}{2} \right)^{2/5} \left( \frac{\mu^*}{\mu_0} \right)^{1/5}$	0

<sup>a</sup>Stratford's model was derived assuming a value of  $\gamma=1.4$ .

and  $a_2$  are determined using the Sutherland viscosity law [25].<sup>4</sup> The largest difference between the laminar boundary layer models of Tang and Geropp occurred at the lowest Reynolds number and was only 0.028%. At the higher Reynolds numbers, the difference monotonically decreased. Between these two models, Geropp's boundary layer model agreed better with measured results and was therefore used for the comparison.

### Inviscid Discharge Coefficient ( $C_{d,2}$ )

Several researchers [17–19] have developed methods for determining the inviscid discharge coefficient. Perhaps, the most widely used model was developed by Hall in 1962. Hall assumed that the gas behaved ideally and had a constant heat capacity. He used a perturbation series expansion in powers of  $1/R$  (where  $R=1/\Omega$ ) to solve the steady, irrotational, axisymmetric, compressible flow equation in the transonic regime [18]. Since the series diverges for  $R < 1$ , it is not unexpected that the accuracy of this solution diminishes for small values of  $R$ . In fact, for sufficiently small  $R$ , Hall's solution yields nonphysical results, predicting negative values of the inviscid discharge coefficient. Consequently, the common practice has been to avoid using this solution for  $R < 2$ . In 1969, Kliegel and Levine [19] extended and improved Hall's work by using a perturbation series solution expanded about  $1/(1+R)$  that converges for all values of  $R$ . In developing the improved series solution, Kliegel and Levine found an error in Hall's original solution and provided the appropriate correction.

The mathematical formulation of the inviscid discharge coefficient is

$$C_{d,2} = 1 - \frac{\alpha_2}{\Lambda^2} + \frac{\alpha_3}{\Lambda^3} - \frac{\alpha_4}{\Lambda^4} \quad (7)$$

where  $\alpha_2$ ,  $\alpha_3$ , and  $\alpha_4$  are species dependent coefficients and  $\Lambda$  is the expansion parameter. Table 4 gives the values of the coefficients and the expansion parameters for Hall's original solution, the corrected version of Hall's solution, and the improved solution of Kliegel and Levine. Figure 6 compares the predicted discharge coefficients given by these three models versus  $\Omega$  for  $\gamma=1.405$ . The left y-axis gives the values of  $C_{d,2}$  for each of the three models, while the right y-axis gives the percent difference between the original series solution of Hall (which unfortunately is still being used by researchers) and the improved series solution of Kliegel and Levine. Within the ISO specified design limits (indicated by the shaded rectangle), the difference between these two solutions is no more than 0.03%, but increases to as much as 0.2% for  $\Omega=0.5$  ( $R=2$ ) with increased differences at larger throat curvature ratios (or smaller  $R$ ).

### Virial Discharge Coefficient ( $C_{d,3}$ )

The virial discharge coefficient is defined as the following ratio of mass flows:

$$C_{d,3} \equiv \frac{\dot{m}_3}{\dot{m}_b} \quad (8)$$

where  $\dot{m}_3$  is the mass flow that would result if the CFV flow was both one dimensional and inviscid, but influenced by virial effects. Unlike the analytical solutions for the viscous and inviscid discharge coefficients previously given in Eqs. (6) and (7), no closed-form solutions have been found that adequately predict  $C_{d,3}$  for arbitrary CFV operating conditions and gas species. Consequently,  $\dot{m}_3$  has been numerically calculated [20] using a real gas equation of state to determine the density and sound speed at the CFV throat. Johnson was the first to make these calculations, and he

<sup>4</sup>The first order terms of the models of Tang and Geropp are identical if the viscosity in Tang's model is taken proportional to temperature, and the ideal gas isentropic relationships are used to relate the throat temperature to the stagnation temperature.

**Table 4 Coefficients and expansion parameter for various series solutions of  $C_{d,2}$** 

Inviscid discharge coefficient ( $C_{d,2}$ )	Series expansion parameter $\Lambda$	Series expansion coefficients		
		$\alpha_2$	$\alpha_3$	$\alpha_4$
Original Hall [18]	$R$	$\frac{\gamma+1}{96}$	$\frac{(\gamma+1)(8\gamma+21)}{4608}$	$\frac{(\gamma+1)(754\gamma^2+1971\gamma+2007)}{552,960}$
Corrected Hall [19]	$R$	$\frac{\gamma+1}{96}$	$\frac{(\gamma+1)(8\gamma+21)}{2304}$	$\frac{(\gamma+1)(754\gamma^2+2123\gamma+2553)}{552,960}$
Kliegel and Levine [19]	$1+R$	$\frac{\gamma+1}{96}$	$\frac{(\gamma+1)(8\gamma-27)}{2304}$	$\frac{(\gamma+1)(754\gamma^2-757\gamma+3633)}{276,480}$

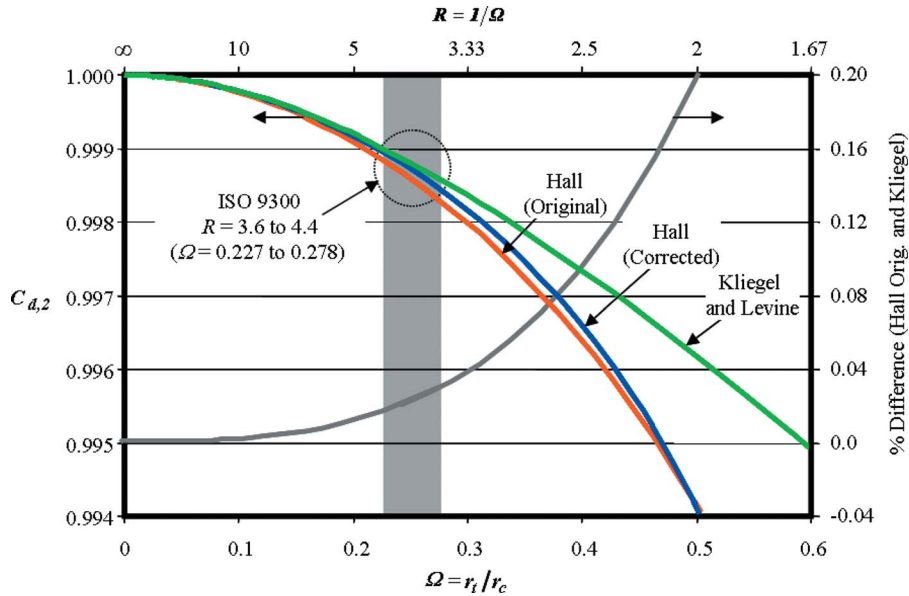


Fig. 6 Comparison of three models of the inviscid discharge coefficient

expressed  $\dot{m}_3$  in a form analogous to the base line model given in Eq. (1).

$$\dot{m}_3 = \frac{\pi d^2 P_0 C_r^* \sqrt{\mathcal{M}}}{4 \sqrt{R_u T_0}} \quad (9)$$

with the sole difference being that  $C_i$  is replaced by  $C_r^*$ . Thus, all real gas effects are lumped into the real gas critical flow function ( $C_r^*$ ), which is a function of  $P_0$ ,  $T_0$  for a given gas species. Subsequently, the virial discharge coefficient is a function of the specific heat ratio, stagnation conditions, and gas species, and can be expressed as the ratio of the real gas critical flow factor and the ideal critical flow factor by substituting Eqs. (1) and (9) into Eq. (8).

$$C_{d,3} = \frac{C_r^*}{C_i^*} \quad (10)$$

### Combining the Theoretical Models to Predict the Measured Discharge Coefficient

Throughout the years, researchers have combined  $C_{d,1}$ ,  $C_{d,2}$ , and  $C_{d,3}$  in various ways to estimate the ideal discharge coefficient ( $C_d^i$ ).<sup>5</sup> In special cases where two of the three conditions comprising the sonic assumption are satisfied,  $C_d^i = C_{d,k}$ , where  $k=1, 2$ , or  $3$  as appropriate based on the relevant flow physics. For example, if both viscous effects and real gas behavior are negligible relative to the effect of the sonic line curvature, then  $C_d^i = C_{d,2}$ , and the two remaining theoretical discharge coefficients,  $C_{d,1}$  and  $C_{d,3}$ , are both unity. However, in cases where all three conditions of the sonic line assumption are simultaneously not satisfied, the ideal discharge coefficient is

$$C_d^i = f(C_{d,1}, C_{d,2}, C_{d,3}) \quad (11)$$

assumed to be a function of all three theoretical discharge coefficients.

Historically, the functional form of  $f$  has been assumed (without justification) to be either a product [24] or a linear combination [17] of the theoretical discharge coefficients  $C_{d,1}$ ,  $C_{d,2}$ , and

<sup>5</sup>Since the theoretical models are corrections for the base line model, from which the ideal discharge coefficient is defined, these models describe  $C_d^i$  and not  $C_d^r$ .

$C_{d,3}$ , respectively. In this work, we expand  $f$  using a Taylor series centered about the base line flow conditions for which all three of the theoretical discharge coefficients are unity. The zeroth and first order terms of the series are defined equal to  $C_d^i$ , while the second order terms are used to estimate how accurately the zeroth and first order terms approximate  $C_d^i$ .

Before deriving the functional form of  $f$ , we introduce two mathematical properties of  $f$  essential to the analysis. The two properties are the following:

- (1)  $f(1, 1, 1) = f_b = 1$  and
- (2)  $C_{d,1} = f(C_{d,1}, 1, 1)$ ,  $C_{d,2} = f(1, C_{d,2}, 1)$ , and  $C_{d,3} = f(1, 1, C_{d,3})$

Both properties logically follow from the definition of the ideal discharge coefficient. The first property expresses the fact that the three theoretical discharge coefficients and  $C_d^i$  are unity when the sonic assumption is satisfied. The second property demonstrates that  $C_d^i$  is completely described by a single theoretical discharge coefficient whenever any two conditions of the sonic assumption are satisfied. By expanding the function  $f(C_{d,1}, C_{d,2}, C_{d,3})$  in a Taylor series centered about the unity base line conditions, we obtain

$$C_d^i = f_b - \sum_{k=1}^3 \left( \frac{\partial f}{\partial C_{d,k}} \right)_b \Delta C_{d,k} + \text{higher order terms} \quad (12)$$

where  $f_b$  and  $(\partial f / \partial C_{d,k})_b$  are the zeroth and first order Taylor coefficients, the subscript  $b$  indicates the unity base line condition, the higher order terms are the truncated terms of the series, and  $\Delta C_{d,k}$  is the departure from unity of the  $k$ th theoretical discharge coefficient defined by

$$\Delta C_{d,k} \equiv 1 - C_{d,k} \quad (13)$$

for  $k=1, 2$ , and  $3$ . Based on Property (1), the first term on the right hand side of Eq. (12) equals unity (i.e.,  $f_b=1$ ). By taking the appropriate partial derivatives of Property (2), the partial derivatives in the second term in Eq. (12) are unity for  $k=1, 2$ , and  $3$ , respectively. When Properties (1) and (2) are applied together, Eq. (12) simplifies to

$$C_d^i = 1 - \Delta C_{d,1} - \Delta C_{d,2} - \Delta C_{d,3} + \text{higher order terms} \quad (14)$$

In the special case where real gas behavior is negligible (i.e.,  $\Delta C_{d,3}=0$ ), the result of Eq. (14) (ignoring the higher order terms)

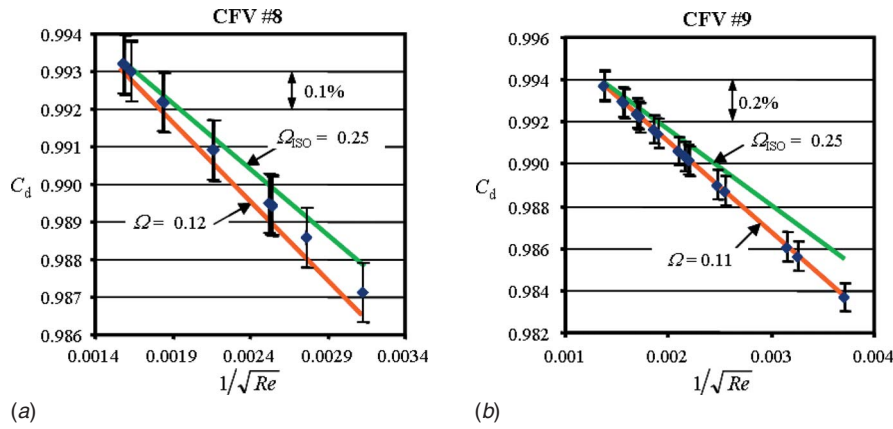


**Fig. 7 Measured discharge coefficient of CFVs 8 (left) and CFV 9 (right) versus predicted  $C_d$  values calculated using their measured  $\Omega$ 's and an assumed value equal to  $\Omega_{ISO}=0.25$**

is consistent with the expression derived by Massier et al. who arrived at this result using an entirely different approach [23]. Without any loss in the order of accuracy, Eq. (14) can be factored into the following form:

$$C_d^i = (1 - \Delta C_{d,1})(1 - \Delta C_{d,2})(1 - \Delta C_{d,3}) + \text{higher order terms} \quad (15)$$

Given that each term in parentheses ( $C_{d,k} \equiv 1 - \Delta C_{d,k}$ ) is equal to one of the three theoretical discharge coefficients,  $C_d^i$  equals

$$C_d^i = C_{d,1}C_{d,2}C_{d,3} + \text{higher order terms} \quad (16)$$

a product of the theoretical discharge coefficients. This multiplicative characteristic of  $C_d^i$  is the basis for introducing a new definition of the discharge that is independent of virial effects. In particular, virial effects are nearly eliminated by defining the real discharge coefficient, which is equal to  $C_d^i$  divided by  $C_{d,3}$ ,

$$C_d \equiv \frac{C_d^i}{C_{d,3}} = C_{d,1}C_{d,2} + \text{higher order terms} \quad (17)$$

The ratio  $C_d^i/C_{d,3}$  is recognized as the real discharge coefficient by recalling from Eq. (10)  $C_{d,3} = C_r^*/C_i^*$  and by using the definition of the real discharge coefficient given in Eq. (4). Because the discharge coefficient as defined in Eq. (17) equals the product of  $C_{d,1}$  and  $C_{d,2}$ , which both by definition are independent of virial effects,  $C_d$  is also independent of virial effects (at least to the accuracy of the higher order terms).

In practice, the definition of the real gas discharge coefficient as given in Eq. (4) is commonly taken to be independent of virial effects. However, virial effects can influence  $C_d$  via the higher order terms in Eq. (17). Physically, the higher order terms account for weak coupling between viscous effects, curvature of the sonic line, and virial effects. The magnitude of the higher order terms can be characterized using only the second order terms and not the entire infinite series since  $|\Delta C_{d,k}| < 1$  for  $k=1, 2$ , and 3. Furthermore, only a subset of the second order terms is necessary to characterize the error in  $C_d$  associated with decoupling virial effects and flow processes. We estimate the magnitude (in percent  $C_d$  change) of this error by

$$\xi_{\text{vir}} = 100 \left[ \frac{|\Delta C_{d,2}\Delta C_{d,3}| + |\Delta C_{d,1}\Delta C_{d,3}|}{C_d} \right] \quad (18)$$

where the first term in the brackets accounts for coupling between virial and boundary layer effects and the second term accounts for coupling between virial effects and sonic line curvature. Since Taylor coefficients of the same variable can be shown to be zero by using Properties (1) and (2), there are no squared terms in-

cluded in the expression. Unfortunately, Properties (1) and (2) are insufficient to determine Taylor coefficients of mixed variables, which are herein assumed to be unity,  $(\partial^2 f / \partial C_{d,k} \partial C_{d,3})_b = 1$  for  $k=1$  and 2. If these coefficients could be determined, a second order correction could be given for  $C_d$ . As it stands, Eq. (18) only estimates the size of the error introduced when  $C_r^*$  is used to reduce real gas behavior in the definition of the discharge coefficient.

Since the three theoretical discharge coefficients are generally close to unity,  $\xi_{\text{vir}}$  is typically small so that  $C_d$  is nearly independent of virial effects. However, in cases where  $\xi_{\text{vir}}$  becomes significant, it should be included in the uncertainty budget.<sup>6</sup> We suggest treating this term as a rectangular distribution [12,13] and including its uncertainty contribution with the uncertainty components of  $C_r^*$ . For the results presented in this paper, this term is insignificant, being less than  $\xi_{\text{vir}} < 0.003\%$ .

## Results

The overall agreement between the measured and predicted discharge coefficients of nine standardly manufactured CFVs was better than 0.17% over a Reynolds number range extending from  $7.2 \times 10^4$  to  $2.5 \times 10^6$ . The best agreement was found for CFVs 8 and 9. The predicted discharge coefficients for these CFVs agreed with measured values to better than 0.065% over a Reynolds number range extending from  $7.2 \times 10^4$  to  $5.0 \times 10^5$ . Figure 7 shows the measured data ( $\blacklozenge$ ) and two  $C_d$  predictions (solid lines), one calculated using the measured value of  $\Omega$  for the CFV, and the other using an assumed value based on ISO guidelines ( $\Omega_{ISO} = 0.25$ ). Both predicted values of the discharge coefficient in the figure are determined by using Eq. (17) (with the higher order terms omitted). We used the boundary layer model of Geropp for the laminar flow and the model of Stratford for the turbulent flow along with the inviscid flow model of Kliegel and Levine. Following the results of the laminar boundary layer models, the  $C_d$  values in the figure are plotted versus  $1/\sqrt{Re}$  to linearize the laminar calibration data.

The results show that reasonably accurate values of  $\Omega$  are needed (i.e., better than 10%) to obtain the best agreement between predicted and measured  $C_d$  values. In Fig. 7, CFV 9 (right) has a curvature ratio ( $\Omega_9=0.11$ ) that is significantly less than ISO recommended values. Given that this CFV was supposed to be machined according to ISO specifications, we were surprised to find that its curvature ratio deviated from the design limit by more

<sup>6</sup>Errors associated with virial effects only apply when CFV calibrations performed using one gas are applied to a different gas.

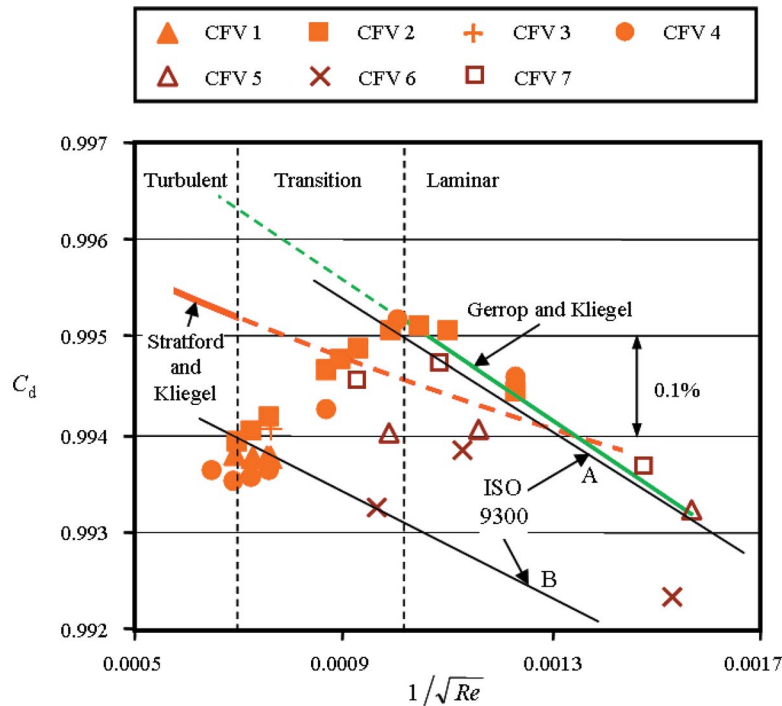


**Fig. 8 Measured discharge coefficient of CFVs 1–7 compared to the piecewise theoretical model spanning the laminar, transition, and turbulent flow regimes (curves labeled A and B are the values of the discharge coefficient recommended by the ISO 9300 standard for accurately and normally machined CFVs [2])**

than 100%. If we had not measured  $\Omega$ , but instead used an assumed ISO value of  $\Omega_{ISO}=0.25$ , the resulting error would have been almost 0.21% at the lowest Reynolds number. In contrast, when we used the measured value of  $\Omega$  in the predictive model, the agreement with calibration data was better than 0.01%.

Applying the measured value of the curvature ratio ( $\Omega_8=0.12$ ) for CFV 8 (left) did not yield a substantial improvement over using an assumed value of  $\Omega_{ISO}=0.25$ . Defects in the geometry of this CFV are probably responsible. In particular, the elliptical shaped cross section of CFV 8 (see Fig. 2) results in a throat radius of curvature that substantially changes at various angles along the throat circumference. Consequently, the uncertainty in the measured throat curvature ratio was 52%. If we hypothetically increased the throat curvature ratio from 0.12 to 0.159, the agreement between theory and measurement would be better than 0.01%. Nevertheless, using the measured  $\Omega$  value yielded results within the calibration uncertainty.

Figure 8 shows the measured  $C_d$ 's for CFVs 1–7 plotted against a piecewise theoretical model that spans the laminar, transition, and turbulent flow regimes. Strictly speaking, the seven different theoretical plots are necessary to account for the geometrical differences (i.e., differing  $\Omega$ ) between the seven CFVs. However, instead of plotting seven different curves, we calculate the theoretical discharge coefficient using a single value of the curvature ratio equal to  $\Omega=0.25$ . This simplification allows a single theoretical curve for all seven CFVs shapes while introducing only 0.023% uncertainty in the predicted discharge coefficient. The dependence on  $\Omega$  is less significant for these larger sized CFVs attributed to the diminished influence of boundary layer effects at higher Reynolds numbers, and because the measured  $\Omega$  of these CFVs (0.18–0.28) is closer to  $\Omega_{ISO}=0.25$ . A further simplification of the theoretical model is the assumption that transition to turbulence occurs at a single Reynolds number,  $Re=10^6$ . As observed in the figure, the actual  $C_d$  data transition from the laminar to the turbulent flow over a Reynolds number range extending from 1

$\times 10^6$  to  $2.1 \times 10^6$ . At  $Re < 10^6$ , the data generally follow a linear trend typical of the laminar flow regime while for  $Re > 2.1 \times 10^6$ , the data appear to be fully turbulent and begin to increase with increasing Reynolds number. Not surprisingly, the simple piecewise model does not capture the downward trend in  $C_d$  that occurs during the transition from the laminar to the turbulent flow.

Excluding CFV 6 which had the largest  $C_d$  uncertainty (see Table 1), the agreement in the laminar regime was better than 0.07%. The worst agreement was in the turbulent regime where the predictive model overestimated the measured data by as much as 0.17%.

In addition to the piecewise theoretical model, we also compared the measured  $C_d$  values to the two ISO 9300 calibration curves for toroidal throat CFVs [2]. In Fig. 8, the ISO 9300 curve labeled A applies to accurately machined CFVs (or HPNs) while the curve labeled B applies to normally manufactured CFVs.<sup>7</sup> The predicted discharge coefficients of both Curves A and B agree with the measured  $C_d$  values within the uncertainties given by ISO 9300 standard of 0.2% and 0.3%, respectively.

## Conclusions

Nine normally manufactured CFVs with nominal diameters ranging from 5 mm to 25 mm were calibrated in dry air, and their measured discharge coefficients agreed with predicted values to better than 0.17% over a Reynolds number range extending from  $7.2 \times 10^4$  to  $2.5 \times 10^6$ . For all nine CFVs, the walls were smooth so that the effect of surface roughness was assumed negligible. The throat diameters ( $d$ ) and the throat curvature ratio ( $\Omega$ ) of

<sup>7</sup>The discharge coefficient for Curve A (i.e., accurately machined CFVs) is  $C_d^A = 0.9985 - 3.412Re^{-0.5}$ , while for Curve B (i.e., normally manufactured CFVs) is  $C_d^B = 0.9959 - 2.720Re^{-0.5}$ . Note that the Reynolds numbers in these expressions are based on the actual mass flow and not on the base line mass flow as previously defined in Eq. (5).

these CFVs were measured using a CMM. The flow calibration results included data in the laminar, transition, and turbulent flow regimes. The theoretical discharge coefficient was determined by combining either Geropp's laminar boundary layer model [16] ( $Re < 10^6$ ) or Stratford's turbulent boundary layer model [17] ( $Re > 10^6$ ) with the inviscid core model of Kliegel and Levine [19].

The best agreement was found in the laminar regime where the difference between measured and predicted discharge coefficients was less than 0.07%. In contrast, the turbulent model over-predicted the measured discharge coefficients by an almost constant offset of 0.14%. Part of the offset could be attributed to the 0.1% uncertainty of the measured data; however, most of the bias is likely attributed to the turbulent model.

The throat curvature ratio ( $\Omega$ ) played an important role for the two smallest CFVs. Dimensional measurements showed that these CFVs had  $\Omega$  that significantly deviated from the intended ISO design value of  $\Omega_{ISO} = 0.25$ . When the predicted discharge coefficient was calculated using the measured values of  $\Omega$ , the results were within the uncertainty of the calibration data. The smallest CFV exhibited the best results, agreeing with the experimental data to better than 0.01%.

The good agreement between measured and predicted  $C_d$ 's gives credibility to using theoretical models to predict the discharge coefficient of geometrically well characterized CFVs with negligible surface roughness. Additional research should be done to investigate what level of agreement can be achieved between measurement and theory in smaller CFVs where high accuracy dimensional measurements are more difficult. Additionally, the predictive models may not be as accurate for smaller CFVs where the Reynolds numbers are lower. In this lower Reynolds number regime (i.e.,  $Re < 5 \times 10^3$ ), the second order terms in the boundary layer models of Tang [15] and Geropp [16] play a larger role, causing the predicted  $C_d$  values of these two models to differ more substantially.

## References

- [1] Wright, J. D., 1998, "The Long Term Calibration Stability of Critical Flow Nozzles and Laminar Flowmeters," *Proceedings of the 1998 NCSL Workshop and Symposium*, Albuquerque, NM, NCSL, pp. 443–462.
- [2] ISO 9300: (E), 1990, "Measurement of Gas Flow by Means of Critical Flow Venturi Nozzles," Geneva, Switzerland.
- [3] Ishibashi, M., Takamoto, M., Watanabe, N., Nakao, Y., and Yokomizo, T., 1994, "Precise Calibration of Critical Nozzles of Various Shapes at the Reynolds Number of  $0.8-2.5 \times 10^5$ ," *Proceedings of Flow Measurement*, Glasgow, UK.
- [4] Ishibashi, M., Morioka, T., and Arnberg, B. T., 2005, "Effect of Inlet Curvature on the Discharge Coefficients of Toroidal-Throat Critical-Flow Venturi Nozzles (Keynote Paper)," *ASME Summer Meeting and Exhibition*, Houston, TX, ASME Paper No. FEDSM2005-77470.
- [5] Ishibashi, M., 2003, "Fluid Dynamics in Critical Nozzles Revealed by Measurements (Keynote Paper)," *Fourth ASME/JSME Joint Fluids Engineering Conference*, Honolulu, HI, ASME Paper No. FEDSM2005-45592.
- [6] Ishibashi, M., 2002, "Super-Fine Structure in the Critical Flow-Rate of Critical Flow Venturi Nozzles," *Joint US-European Fluids Engineering Conference*, Montreal, Canada, ASME Paper No. FEDSM2002-31079.
- [7] Wright, J. D., Johnson, A. N., and Moldover, M. M., 2003, "Design and Uncertainty Analysis for a PVTt Gas Flow Standard," *J. Res. Natl. Inst. Stand. Technol.*, **108**, pp. 21–47.
- [8] Wright, J. D., Moldover, M. R., Johnson, A. N., and Mizuno, A., 2003, "Volumetric Gas Flow Standard With Uncertainty of 0.02% to 0.05%," *ASME J. Fluids Eng.*, **125**(6), pp. 1058–1066.
- [9] Johnson, A. N., and Wright, J. D., 2006, "Gas Flowmeter Calibrations With the 26 m<sup>3</sup> PVTt Standard," *Journal of Research of the National Institute of Standards and Technology*, NIST Special Publication 250-1046.
- [10] Johnson, A. N., Wright, J. D., Moldover, M. R., and Espina, P. I., 2003, "Temperature Characterization in the Collection Tank of the NIST 26 m<sup>3</sup> PVTt Gas Flow Standard," *Metrologia*, **40**, pp. 211–216.
- [11] Stoup, J. R., and Doiron, T. D., 2001, "The Accuracy and Versatility of the NIST M48 Coordinate Measuring Machine," *Proc. SPIE*, **4401**, pp. 136–146.
- [12] Taylor, B. N., and Kuyatt, C. E., 1994, "Guidelines for Evaluating and Expressing the Uncertainty of NIST Measurement Results," NIST TN-1297.
- [13] ISO, 1995, "Guide to the Expression of Uncertainty in Measurement," International Organization for Standardization (ISO), Geneva, Switzerland.
- [14] John, J. E., 1984, *Gas Dynamics*, 2nd ed., Allyn and Bacon, Boston.
- [15] Tang, S., 1969, "Discharge Coefficients for Critical Flow Nozzles and Their Dependence on Reynolds Numbers," Ph.D. thesis, Princeton University, Princeton, NJ.
- [16] Geropp, D., 1971, "Laminare Grenzschichten in Ebenen und Rotationssymmetrischen Lavalduesen," *Deutsche Luft-Und Raumfahrt, Forschungsbericht*, pp. 71–90.
- [17] Stratford, B. S., 1964, "The Calculation of the Discharge Coefficient of Profiled Choked Nozzles and the Optimum Profile for Absolute Air Flow Measurement," *J. R. Aeronaut. Soc.*, **68**, pp. 237–245.
- [18] Hall, I. M., 1962, "Transonic Flow in Two-Dimensional and Axially-Symmetric Nozzles," *Q. J. Mech. Appl. Math.*, **15**, pp. 487–508.
- [19] Kliegel, J. R., and Levine, J. N., 1969, "Transonic Flow in Small Throat Radius of Curvature Nozzles," *AIAA J.*, **7**, pp. 1375–1378.
- [20] Johnson, R. C., 1964, "Calculations of Real-Gas Effects in Flow Through Critical Nozzles," *ASME J. Basic Eng.*, **86**, pp. 519–526.
- [21] Back, L. H., and Cuffel, R. F., 1971, "Flow Coefficients for Supersonic Nozzles With Comparatively Small Radius of Curvature Throats," *J. Spacecraft*, **8**(2), pp. 196–198.
- [22] Smith, R. E., and Matz, R. J., 1962, "A Theoretical Method of Determining Discharge Coefficients for Venturis Operating at Critical Flow Conditions," *ASME J. Basic Eng.*, **84**(4), pp. 434–446.
- [23] Massier, P. F., Back, L. H., Noel, M. B., and Saheli, F., 1970, "Viscous Effects on the Flow Coefficient for a Supersonic Nozzle," *AIAA Technical Note*, pp. 605–607.
- [24] Ishibashi, M., and Takamoto, M., 1997, "Very Accurate Analytical Calculation of the Discharge Coefficients of Critical Venturi Nozzles With Laminar Boundary Layer," *Proceedings of the FLUCOME*, Hayama, Japan, Sept. 14.
- [25] White, F. M., 1991, *Viscous Fluid Flow*, McGraw-Hill, New York.
- [26] Johnson, A. N., Wright, J. D., Nakao, S., Merkle, C. L., and Moldover, M. R., 2000, "The Effect of Vibrational Relaxation on the Discharge Coefficient of Critical Flow Venturis," *Flow Meas. Instrum.*, **11**(4), pp. 315–327.
- [27] Johnson, A. N., 2000, "Numerical Characterization of the Discharge Coefficient in Critical Nozzles," Ph.D. thesis, Pennsylvania State University, University Park, PA.